

Supporting Information

Synergistic Effects of Charge Transport Engineering and Passivation Enabling Efficient Inverted Perovskite Quantum-dot Light-emitting Diodes

Jiangyong Pan,^{a b †} Fan Fang,^{b †} Jing Xie,^c Lixi Wang,^b Jing Chen,^{* b} Jianhua Chang,^a Wei Lei,^{* b} Wei Zhang,^d Dewei Zhao^{* e}

^a School of Electronic & Information Engineering, Nanjing University of Information Science & Technology, Nanjing 210044, P. R. China

^b Joint International Research Laboratory of Information Display and Visualization, School of Electronic Science and Engineering, Southeast University, Nanjing, 210096, P. R. China E-mail: chenjing@seu.edu.cn; lw@seu.edu.cn

^c Department of Materials Science and Engineering, University of Florida, Gainesville, Florida 32611, USA

^d Shenzhen China Star Optoelectronics Semiconductor, Display Technology Co., Ltd., Shenzhen 518132, P. R. China

^e Institute of Solar Energy Materials and Devices, College of Materials Science and Engineering, Sichuan University, Chengdu 610065, P. R. China E-mail: dewei_zhao@hotmail.com and dewei.zhao@scu.edu.cn

[†]These authors contributed equally to this work.

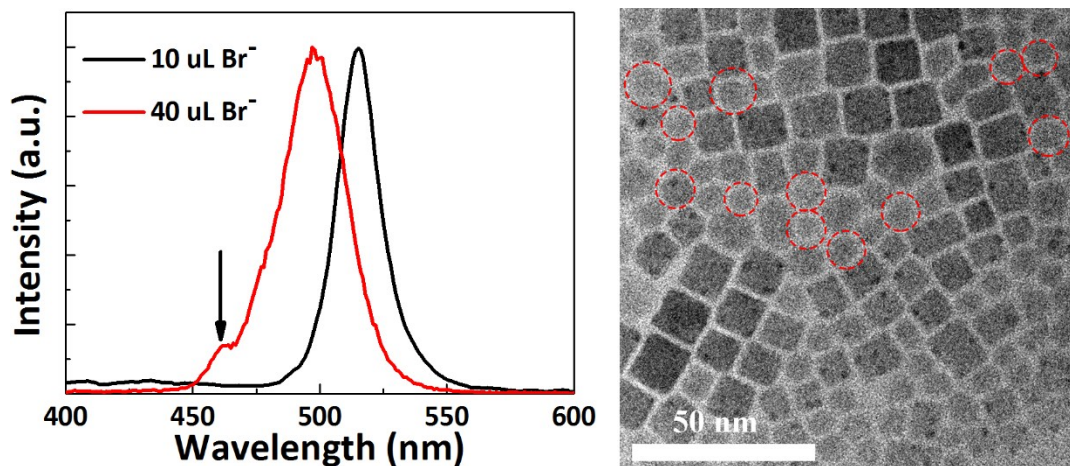


Fig. S1. (a) PL spectra of the CsPbBr₃ with passivation of different amount of bromide anion (b) TEM of the CsPbBr₃ with passivation of excessive bromide anion

When the amount of Br anion is excessive, the PL emission shows an obvious blue shift from 515 to 497 nm along with a parasitic peak located at higher energy region. In addition, the FWHM of PL emission spectrum increases from 19 to 40 nm as shown in Fig. S1a. It can be found that there are small-sized particles re-formed when the Br anion is excessive (Fig. S1b).

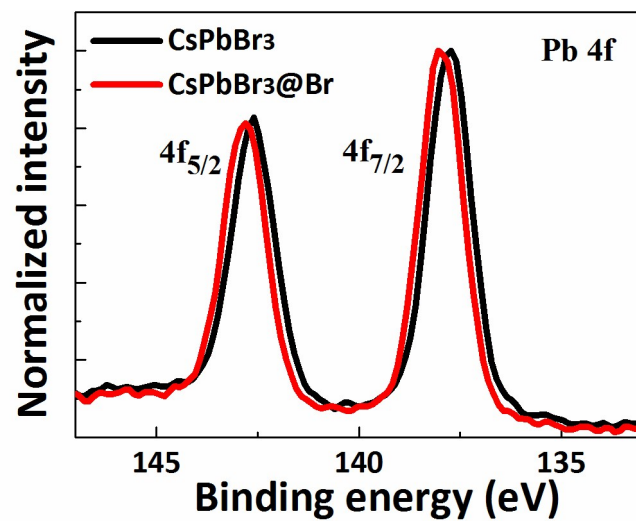


Fig. S2. Pb 4f XPS core level spectra of CsPbBr₃. Spectra of CsPbBr₃@Br show higher binding energy shift by 0.18 eV compared to those of pristine CsPbBr₃.

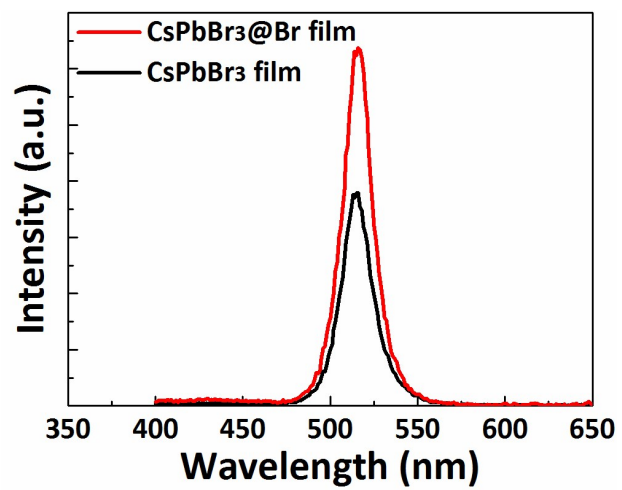


Fig. S3. Steady-state PL spectra of the pristine CsPbBr₃ QDs and post-passivated CsPbBr₃ QDs.

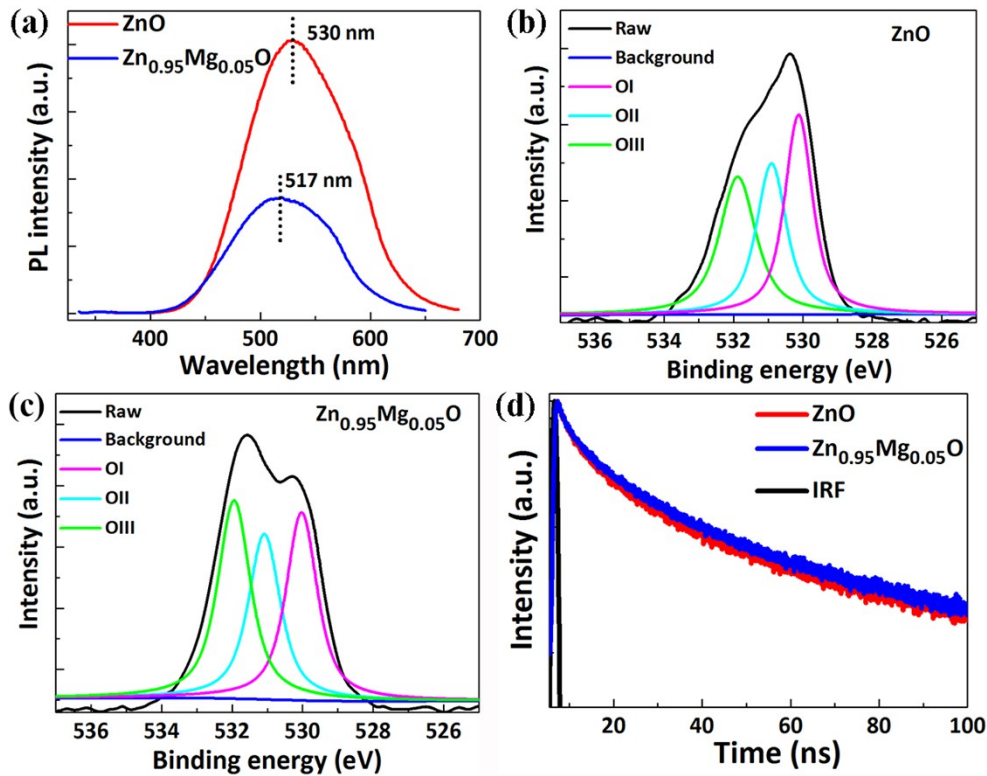


Fig. S4. (a) PL spectra of $\text{Zn}_{0.95}\text{Mg}_{0.05}\text{O}$ and ZnO . O1s XPS spectra of (b) ZnO and (c) $\text{Zn}_{0.95}\text{Mg}_{0.05}\text{O}$. (d) PL decay curves of QDs with a structure of ITO/ZnO or $\text{Zn}_{0.95}\text{Mg}_{0.05}\text{O}/\text{QDs}$

As shown in Fig. S4a, the visible and broad PL emission of ZnO originates from the defect related recombination,¹ and therefore the intensity of visible emission reflects the concentration of defects to some degree. It is found that the intensity of defect related emission peaked at 517 nm is decreased remarkably due to the doping of Mg into ZnO . In addition, defects in metal oxide usually originate from oxygen vacancies.^{2, 3} In order to quantitatively verify the amount of defect composed of oxygen vacancies after doping, the ZnO and $\text{Zn}_{0.95}\text{Mg}_{0.05}\text{O}$ were characterized by XPS and the resulting O1s spectra are shown in Fig. S4 (b-c). The asymmetric O1s peaks of ZnO and $\text{Zn}_{0.95}\text{Mg}_{0.05}\text{O}$ are centered at 529.9 ± 0.1 eV (OI), 531.2 ± 0.1 eV (OII) and 532.0 ± 0.1 eV (OIII), respectively. The OII state is related to the oxygen vacancies.¹ The relative amounts of oxygen vacancies (OII/OI + OII + OIII) are 33.7% and 27.5% for ZnO and $\text{Zn}_{0.95}\text{Mg}_{0.05}\text{O}$, respectively. As a result, this enables us to conclude the defect density is decreased upon Mg doping. The defects such as oxygen vacancies can quench the excitons in QDs via an intragap-assisted nonradiative recombination process.⁴ We performed the TRPL measurement to study the effect of the ZnO and $\text{Zn}_{0.95}\text{Mg}_{0.05}\text{O}$ on the emission quenching of QDs by constructing the films with a structure of ITO/ZnO or $\text{Zn}_{0.95}\text{Mg}_{0.05}\text{O}/\text{QDs}$. It is clear that the exciton lifetimes of the QDs contacting ZnO and $\text{Zn}_{0.95}\text{Mg}_{0.05}\text{O}$ are calculated to be 28.24 and 34.41 ns, respectively (Fig. S4d), indicating the exciton lifetime of the QDs increases due to the suppressed exciton quenching at the $\text{Zn}_{0.95}\text{Mg}_{0.05}\text{O}/\text{QDs}$ interface.

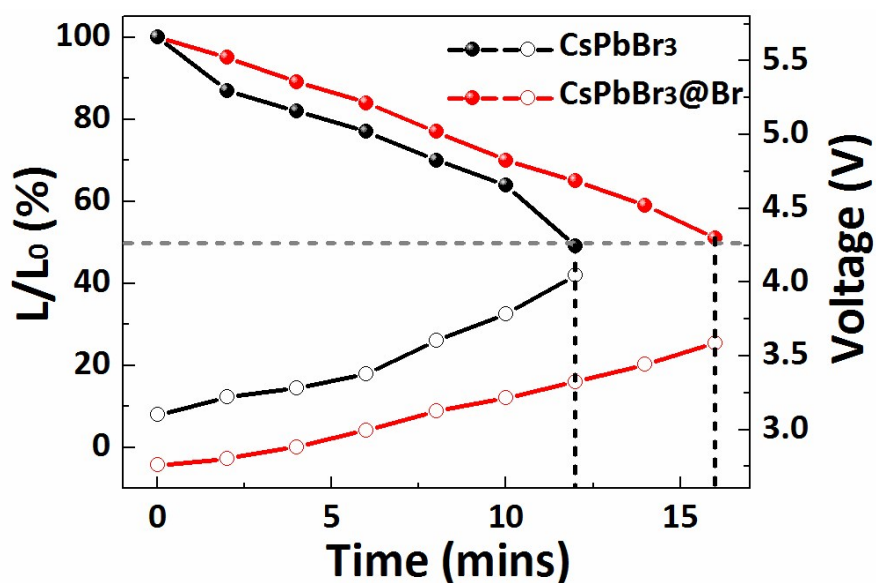


Fig. S5. Operational stability and driving voltage for PVQDLEDs with different QDs under constant driving currents of 4 mA cm^{-2}

The difference in stability between CsPbBr₃- and CsPbBr₃@Br-based devices is displayed in Fig. S5. The lifetime of the CsPbBr₃@Br-based device exceeds 16 min, surpassing that of CsPbBr₃-based device (12 min). In addition, the driving voltage of a CsPbBr₃-based device increases from 3.1 to 4.1 V, while that of CsPbBr₃@Br -based device increases from 2.8 to 3.6 V. The improvement in device stability is ascribed to effective inhibition of ion migration by passivation, since surface defects are considered as the primary path for ion migration.⁵

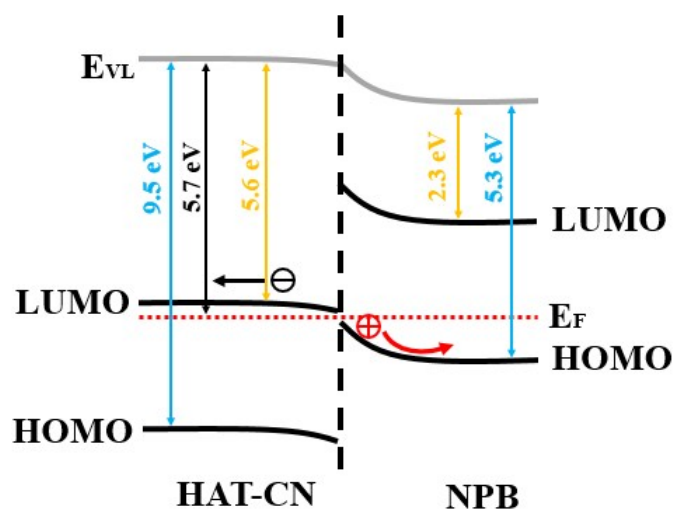


Fig. S6. Energy level in the interface of NPB/HAT-CN

The Fermi level at the interface of NPB/HAT-CN moves down and pins at a certain position as normally occurred by p-doping.^{6,7}

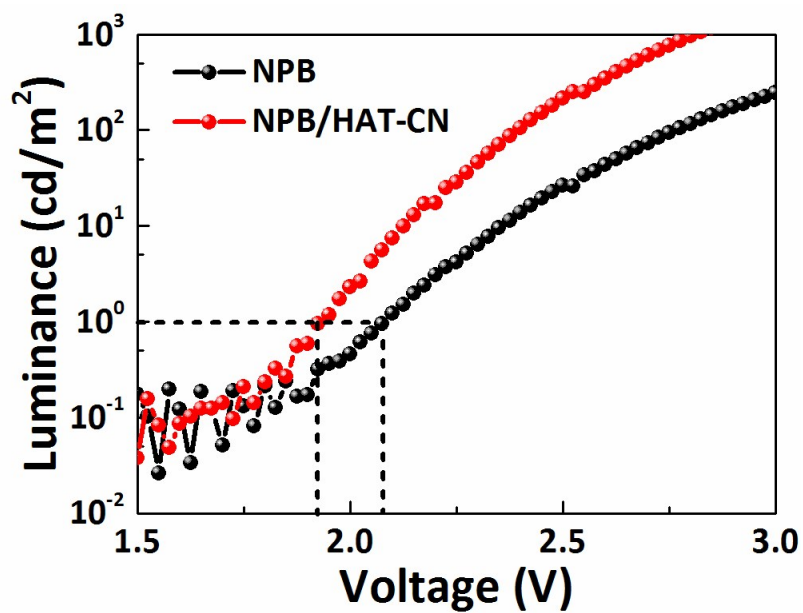


Fig. S7. Enlarged luminance-voltage curve of the devices with NPB and NPB/HAT-CN HTL as a function of driving voltage.

Upon usage of NPB/HAT-CN as HTL, the turn-on voltage (at which the luminance reaches 1 cd m⁻²) of the device decreases from 2.1 to 1.9 V.

Table S1. Fitted PL lifetimes of different QD films measured by using exponential decay: $I(t) = P_1 \times \exp(-t/\tau_1) + P_2 \times \exp(-t/\tau_2) + P_3 \times \exp(-t/\tau_3)$. The average lifetime is calculated by using: $\tau_{ave} = P_1 \times \tau_1 + P_2 \times \tau_2 + P_3 \times \tau_3$

Sample	τ_1 (ns)	τ_2 (ns)	τ_3 (ns)	τ_{ave} (ns)	P_1 (%)	P_2 (%)	P_3 (%)
CsPbBr ₃	1.07	7.80	53.57	35.36	11.10	27.04	61.86
CsPbBr ₃ @Br	2.68	8.65	50.10	27.34	12.60	40.50	46.90

References

1. Y. Sun, Y. Jiang, H. Peng, J. Wei, S. Zhang and S. Chen, *Nanoscale*, 2017, **9**, 8962-8969.
2. B. S. Mashford, M. Stevenson, Z. Popovic, C. Hamilton, Z. Q. Zhou, C. Breen, J. Steckel, V. Bulovic, M. Bawendi, S. Coe-Sullivan and P. T. Kazlas, *Nat. Photonics*, 2013, **7**, 407-412.
3. Y. Y. Tay, T. T. Tan, M. H. Liang, F. Boey and S. Li, *Phys. Chem. Chem. Phys.*, 2010, **12**, 6008-6013.
4. Q. Su, H. Zhang, Y. Sun, X. W. Sun and S. Chen, *ACS Appl. Mater. Interfaces*, 2018, DOI: 10.1021/acsami.8b08470.
5. M. Abdi-Jalebi, Z. Andaji-Garmaroudi, S. Cacovich, C. Stavarakas, B. Philippe, J. M. Richter, M. Alsari, E. P. Booker, E. M. Hutter, A. J. Pearson, S. Lilliu, T. J. Savenije, H. Rensmo, G. Divitini, C. Ducati, R. H. Friend and S. D. Stranks, *Nat.*, 2018, **555**, 497-501.
6. Y. Tao, C. Yang and J. Qin, *Chem. Soc. Rev.*, 2011, **40**, 2943-2970.
7. S. M. Park, Y. H. Kim, Y. Yi, H.-Y. Oh and J. Won Kim, *Appl. Phys. Lett.*, 2010, **97**, 063308.